

Interaction Analyses of the Integrin β2 Cytoplasmic Tail with the F3 FERM Domain of Talin and 14-3-3ζ Reveal a Ternary Complex with Phosphorylated Tail

Deepak Chatterjee, Lewis Lu Zhiping, Suet-Mien Tan and Surajit Bhattacharjya

School of Biological Sciences, *Nanyang Technological University, 60 Nanyang Drive, Singapore 637551, Singapore*

Correspondence to Suet-Mien Tan and Surajit Bhattacharjya: *60 Nanyang Drive, Singapore 637551, Singapore.*
smtan@ntu.edu.sg; surajit@ntu.edu.sg
http://dx.doi.org/10.1016/j.jmb.2016.08.014
Edited by James Sellers

Abstract

Integrins, which are heterodimeric (α and β subunits) signal-transducer proteins, are essential for cell adhesion and migration. β cytosolic tails (β-CTs) of integrins interact with a number of cytosolic proteins including talin, Dok1, and 14-3-3ζ. The formation of multiprotein complexes with β-CTs is involved in the activation and regulation of integrins. The leukocyte-specific β2 integrins are essential for leukocyte trafficking, phagocytosis, antigen presentation, and proliferation. In this study, we examined the binding interactions between integrin β2-CT and T758-phosphorylated β2-CT with positive regulators talin and 14-3-3ζ and negative regulator Dok1. Residues of the F3 domain of talin belonging to the C-terminal helix, β-strand 5, and the adjacent loop were found to be involved in the binding interactions with β2-CT. The binding affinity between talin F3 and β2-CT was reduced when β2 T758 was phosphorylated, but this modification promoted 14-3-3ζ binding. However, we were able to detect stable ternary complex formation of T758-phosphorylated β2-CT, talin F3, and 14-3-3ζ that involved the repositioning of talin F3 on β2-CT. We showed that Dok1 binding to β2-CT was reduced in the presence of 14-3-3ζ and when β2 T758 was phosphorylated. Based on these data, we propose a sequential model of β2 integrin activation involving these molecules. Our study provides for the first time insights toward β2 integrin activation that involves a multiprotein complex.
© 2016 Elsevier Ltd. All rights reserved.

Introduction

Integrins are transmembrane receptors that mediate cell–cell and cell–extracellular matrix adhesions [1]. Integrins are obligate heterodimers composed of non-covalently linked α and β subunits. Each subunit contains a large extracellular domain, a single-pass transmembrane domain, and a short cytoplasmic tail (CT) [1]. Integrin inside-out activation is a process by which the disruption of the interface between the membrane-proximal (MP) regions of the α and β subunits and the cytoplasmic tails leads to the separation of their transmembrane domains, followed by global conformational changes in the extracellular regions [2]. The integrin β-CTs, excluding β4 and β8, contain two highly conserved NPxY/F motifs. Both motifs are docking sites for cytoplasmic proteins that regulate integrin activation [3].

Talin-1 (henceforth referred to as talin) is a large cytoskeletal protein composed of a 4.1-ezrin-radixin-moesin (FERM)-containing head region and a long rod region [4]. Talin is a well-established positive regulator of integrin activation. It binds directly to the integrin β-CTs and disrupts the MP interface of the cytoplasmic tails [5]. The phosphotyrosine binding (PTB) fold in the F3 subdomain of talin binds to the MP NPxY/F motif of the integrin β-CT [6]. It has been reported that the phosphorylation state of the integrin β3 MP NPLY functions as a switch that regulates the binding of either talin or Dok1, a cytoplasmic negative regulator of integrin activation [7]. Recently, it has been demonstrated that an alternative phosphorylation switch involving two Ser residues flanking the integrin β2 MP NPLF motif served a similar function [8]. These data exemplify the relevance of integrin β tail post-translational modification(s) as a part of the mechanism by which fine-tuned regulation of integrin activation could be achieved.

The leukocyte-restricted integrin β2 subfamily contains four members that share a common β2

© 2016 Elsevier Ltd. All rights reserved.

subunit, namely αLβ2, αMβ2, αXβ2, and αDβ2 [3]. The β2-CT contains a triplet Thr motif that lies in between its two NPxF motifs. The phosphorylation status of this triplet Thr motif modulates the association of the integrin β2-CT with cytoplasm proteins. 14-3-3 family of proteins is known to bind pSer/Thr-containing sequences, and they form dimers [9–11]. 14-3-3ζ binds the pTTT motif in the integrin β2-CT, and it serves as a positive regulator of β2 integrin-ligand binding [12,13]. Structural data revealed a 14-3-3ζ homodimer in complex with two pTTT-containing integrin β2 tail peptides, suggesting that 14-3-3ζ can positively regulate β2 integrins functions by promoting receptor clustering [14]. Notably, the same study also showed that the phosphorylation of Thr758 (the first residue of the triplet Thr) in the integrin β2-CT promotes 14-3-3ζ but inhibits filamin binding [14]. Phosphorylation of the triplet Thr in the integrin β7-CT has also been shown to reduce filamin binding, a negative regulator of integrin activation, but not talin binding [15]. Furthermore, β2-CT phosphorylation of residue S756 close to the NPLF754 and T^{758}TT motif recruits Dok1, a negative regulator of integrin activation [8]. Taken together, phosphorylation of the triplet Thr motif and adjacent Ser756 in the integrin β2-CT serves like a switch that regulates the docking of 14-3-3ζ, filamin A, and Dok1 with opposing functions with respect to integrin activation.

Mechanistically, the dissociation of filamin A from the integrin β-CT, followed by the docking of positive regulators such as 14-3-3ζ and talin, is well rationalized and supported by available data. However, it remains to be clarified if 14-3-3ζ, talin, and Dok1 with binding sites that are close to each other on integrin β2-CT can form ternary complexes or if their interactions with the integrin β2-CT are mutually exclusive. There is also limited information on how the phosphorylation of the triplet Thr in the integrin β2-CT regulates the binding of 14-3-3ζ in the presence of talin and vice versa. In this work, we set out to understand the interactions among talin F3 domain, 14-3-3ζ, and Dok1 with β2-CT. Our results showed that talin F3 domain exhibits different affinities for β2-CT and pTβ2-CT by employing residues located at the C-terminal long helix, β-strand 5, and the adjoining loop region. Ternary complex formation of 14-3-3ζ, talin F3 domain, and pTβ2-CT was examined. Based on the docked structure of the ternary complex, the MP helix of pTβ2-CT interacts with the talin F3 domain, and its C-terminal region containing residue pT758 occupies the canonical binding pocket of 14-3-3ζ. These results provide important insights for multiprotein complex formation between β2-CT and its interacting partners that are relevant to the activation mechanism of β2 integrins.

Results

The F3 domain of talin interacted with β2-CT using the canonical binding pocket

Backbone ^{15}N–^{1}H correlations of talin F3 were assigned by combined analyses of 3D HNCACB and CBCA(CO)NH spectra. A series of ^{15}N–^{1}H HSQC spectra of F3 were acquired in the presence of different concentrations and molar ratios, 1:0, 1:0.4, 1:0.8, 1:1.2, 1:1.6, 1:2, 1:3, 1:4, and 1:5, of synthetic β2-CT. Table 1 provides a list of synthetic β2-CTs used in this study. ^{15}N–^{1}H HSQC spectra overlay of talin F3 in free solution (blue contour) and in the presence of β2-CT at 1:1 (red contour) and 1:3 (brown contour) molar ratios is shown (Fig. 1a). ^{15}N–^{1}H HSQC spectra of talin F3 showed chemical shift changes and also the broadening of resonances that suggest binding interactions. Residues of talin F3 located at the central segment (e.g., E350, W351, L353, T354, and N355) and a continuous stretch of C-terminal region (e.g., A^{389}QLIAGY^{395}) exhibited pronounced chemical shift changes in the presence of β2-CT (Fig. 1b). Additionally, ^{15}N–^{1}H cross-peaks of a number of residues at the central region of talin F3 were broadened due to its binding to β2-CT (Fig. 1b). An apparent dissociation constant (K_d) value of 243.8 μM of talin F3/β2-CT complex was estimated from the chemical shift changes of talin F3 (Fig. 1c and Table 2). The β2-CT-induced chemical shift changes (>0.04 ppm) and resonance broadening effect were mapped onto the 3D structure of talin F3 (Fig. 1d). The 3D

Table 1. Primary structures of synthetic β2-CT and β2-CT peptide fragments used in this study

Name	Residues	Sequence
β2-CT	724–769	K-A-L-I-H-L-S-D-L-R-E-Y-R-R-F-E-K-E-K-L-K-S-Q-W-N-N-D-N-P-L-F-K-S-A-T-T-T-V-M-N-P-K-F-A-E-S
pTβ2-CT	724–769	K-A-L-I-H-L-S-D-L-R-E-Y-R-R-F-E-K-E-K-L-K-S-Q-W-N-N-D-N-P-L-F-K-S-A-**pT**-T-T-V-M-N-P-K-F-A-E-S
pTDS20	751–769	D-N-P-L-F-K-S-A-**pT**-T-T-V-M-N-P-K-F-A-E-S
KS33	724–757	K-A-L-I-H-L-S-D-L-R-E-Y-R-R-F-E-K-E-K-L-K-S-Q-W-N-N-D-N-P-L-F-K-S
pTβ2WA	724–769	K-A-L-I-H-L-S-D-L-R-E-Y-R-R-F-E-K-E-K-L-K-S-Q-**A**-N-N-D-N-P-L-F-K-S-A-**pT**-T-T-V-M-N-P-K-F-A-E-S
pTβ2FA	724–769	K-A-L-I-H-L-S-D-L-R-E-Y-R-R-F-E-K-E-K-L-K-S-Q-W-N-N-D-N-P-L-**A**-K-S-A-**pT**-T-T-V-M-N-P-K-F-A-E-S
pSpTβ2-CT	724–769	K-A-L-I-H-L-S-D-L-R-E-Y-R-R-F-E-K-E-K-L-K-S-Q-W-N-N-D-N-P-L-**A**-K-**pS**-A-**pT**-T-T-V-M-N-P-K-F-A-E-S

Phosphorylated residues and Ala replacements are set in boldface.

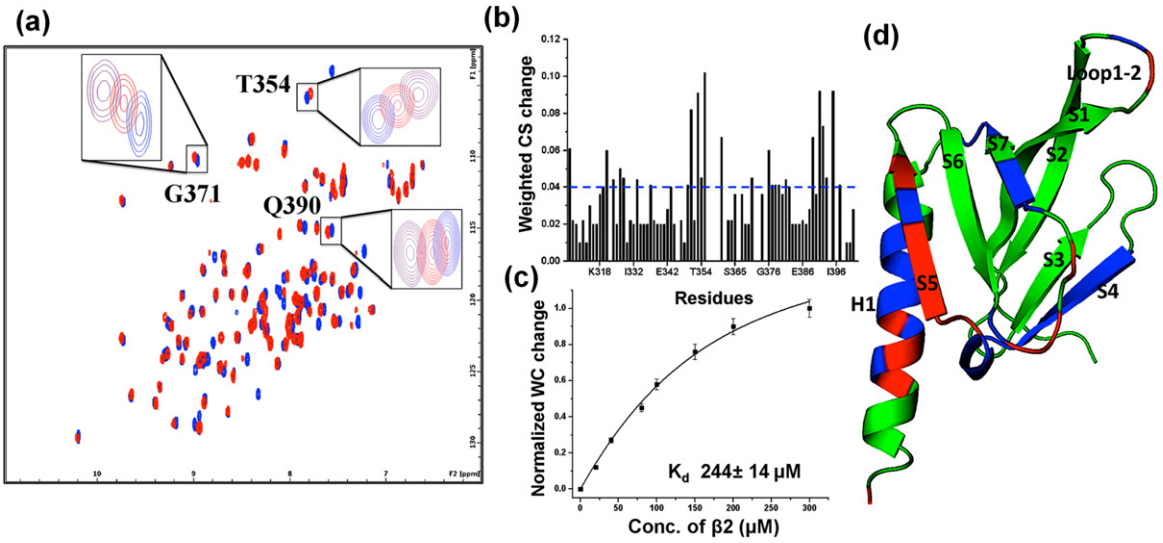


Fig. 1. Mapping talin F3 interactions with β2-CT. (a) Overlay of ^{15}N–^{1}H HSQC spectra of talin F3 in the absence of β2-CT (blue contour) and in the presence of increasing concentrations of β2-CT at 1:1 (red contour) and 1:3 (brown contour) ratios. Chemical shift changes of some representative residues T354, G371, and Q390 are highlighted. (b) Bar diagram showing combined CSP for ^{15}N and HN resonances of each residue of talin F3 upon binding to β2-CT at F3:β2-CT 1:3 ratio. The dotted line marked average CSP. (c) Normalized chemical shift differences are plotted against the concentrations of β2-CT for talin F3 to determine equilibrium dissociation constant (K_d) value. (d) A ribbon representation of the 3D structure of talin F3. Residues that exhibited above average CSPs and resonance broadening in the presence of β2-CT are shown as blue and red, respectively.

structure of talin F3 represents a canonical PTB fold, whereby the C-terminal long helix and the adjacent β-strands including loops may be involved in the interactions with β2-CT (Fig. 1d). ^{15}N–^{1}H HSQC titrations were also carried out for ^{15}N-labeled β2-CT with unlabeled talin F3 protein. ^{15}N–^{1}H HSQC spectra of β2-CT in complex with F3 domain revealed perturbation of most of the residues (Supplementary Fig. S1). Residues of the β2-CT with >90% signal attenuation when in complex with talin F3 domain are shown (Fig. 2a). Residues located in both the MP helix and the membrane-distal (MD) β-strand of β2-CT were perturbed upon binding to talin F3. Based on chemical shift perturbations (CSPs), a molecular docked model of talin F3 and β2-CT was generated (Fig. 2b). In the docked structure, the β2-CT interacts through its MP helical region and residues at the MD loop with talin F3.

Table 2. Determination of K_d values of β2-CT, pTβ2-CT, talin F3, and 14-3-3ζ interactions by ^{15}N–^{1}H HSQC titrations

Complex	K_d (μM)
^{15}N-F3/β2-CT	244 ± 14
^{15}N-F3/pTβ2-CT	578 ± 74
^{15}N-F3/pTβ2-WA	1361 ± 248
^{15}N-F3/pTβ2-FA	668 ± 75
^{15}N-F3/KS33	357 ± 31
^{15}N-F3/14-3-3ζ/pTβ2-CT	213 ± 25
^{15}N-F3/14-3-3ζ/pTβ2 FA	493 ± 61
^{15}N-F3/14-3-3ζ/pTβ2 WA	564 ± 62

The overall topology of the β2-CT/talin F3 docked structure resembles well with the structures of β1D-CT/talin 2 F2/F3 complex [16] and β3 hybrid CT/talin/F3 complex [17]. Notably, the MP helix of β2-CT demonstrated potential ionic interactions involving the residue D731/K316 and the non-polar packing of residuesY735/L325 and F738/P363 (Fig. 2b). Furthermore, packing interactions with talin F3 can be seen for residues of the MD part of β2-CT, for example, W747/Y377, W747/W359, L753/I396, and L753/L400 (Fig. 2b).

Thr758 phosphorylation of β2-CT modulated its binding with talin F3

Phosphorylation of residues in β-CTs modulates its binding affinity with talin and other interacting proteins [7,8,14,18]. Residue Thr758 in the TTT motif of β2-CT is known be phosphorylated, and it allows the binding of 14-3-3ζ protein to the β2-CT. However, the consequence of β2-CT Thr758 phosphorylation on its binding to talin remains unclear. ^{15}N–^{1}H HSQC spectra of talin F3 were acquired at F3:pTβ2-CT molar ratios of 1: 0, 1:0.4, 1:0.8, 1:1.2, 1:1.6, 1:2, 1:3, 1:4, and 1:5. Figure 3a shows the chemical shift changes of residues of talin F3 in the presence of pTβ2-CT at 1:3 M ratio. Residues in the talin F3 central β-sheet and C-terminal helical region showed resonance perturbation in the presence of pTβ2-CT, akin to interactions with the non-phosphorylated β2-CT. However, most of the

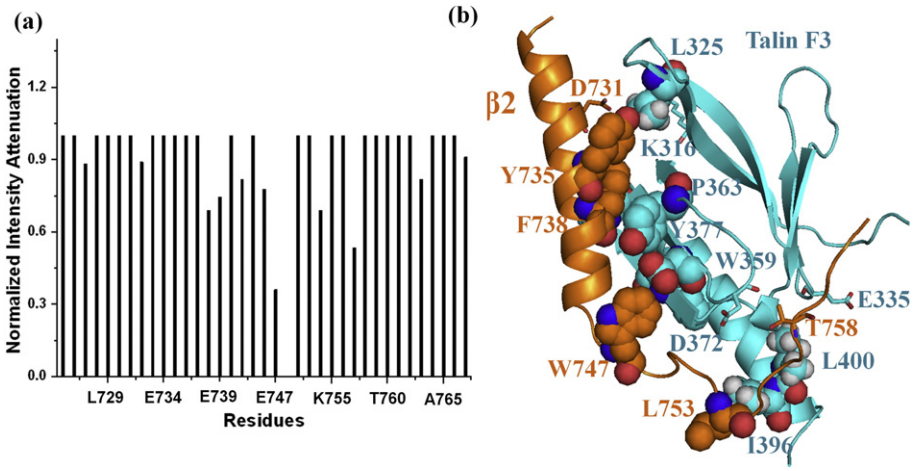


Fig. 2. Interactions of β2-CT with talin F3 and F3/β2-CT docked **complex.** (a) A bar diagram showing the change of intensity in $^{15}N–^{1}H$ HSQC spectra of β2-CT upon the addition of talin F3 at 1:3 ratio. (b) A ribbon representation of the docked structure of talin F3 (cyan) and β2-CT (light red) highlighting some of the residues at the interface of the complex.

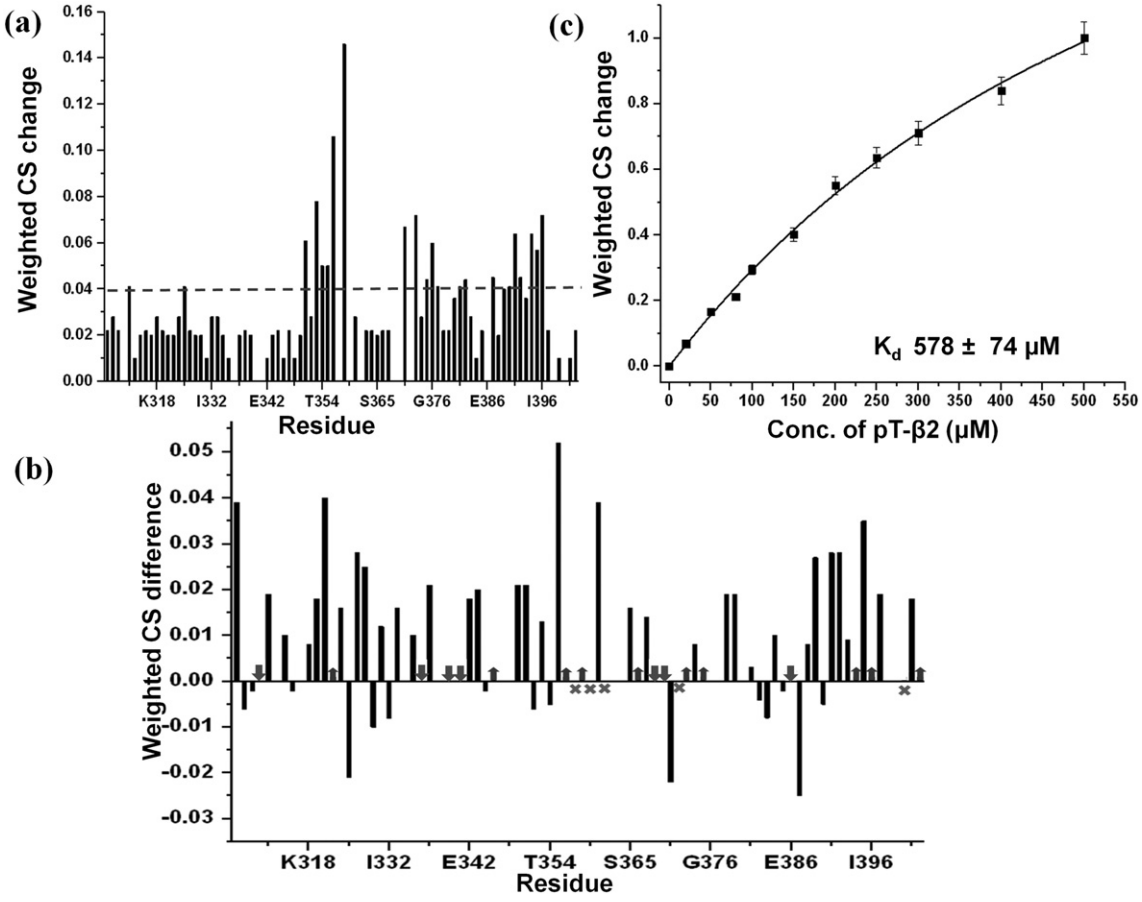


Fig. 3. Mapping talin F3 interactions with pTβ2-CT. (a) Bar diagram showing combined CSP for ^{15}N and HN resonances of each residue of talin F3 upon binding to β2-CT at F3:β2-CT 1:3 ratio. The dotted line marked average CSP. (b) Bar diagram showing differences in weighted chemical shift of residues of F3 talin in the presence of β2-CT and pTβ2-CT. $^{15}N–^{1}H$ HSQC cross-peaks of some residues of F3 delineated resonance broadening upon binding interactions with either β2-CT or pTβ2-CT are marked as down arrows and up arrows, respectively. Residues of F3 showing resonance broadening upon binding interactions with β2-CT and pTβ2-CT are indicated as cross. (c) Normalized chemical shift differences are plotted against the concentrations of pTβ2-CT for talin F3 to determine the equilibrium dissociation constant (K_d) value.

residues of talin F3 showed a lower extent of chemical shift changes in the presence of pTβ2-CT compared to the β2-CT (Fig. 3b). It should also be noted that different residues of talin F3 exhibited the broadening of $^{15}N–^{1}H$ HSQC cross-peaks while interacting with β2-CT and pTβ2-CT, indicating conformational exchange processes (Fig. 3b). Regardless, an apparent K_d value of F3/pTβ2-CT interactions was estimated to be 578 μM from the chemical shift binding curve (Fig. 3c and Table 2). The docked structure of talin F3/β2-CT revealed the close proximity of residue T758 with negatively charged residues D372 and E335 of talin F3 (Fig. 2b). Therefore, phosphorylation of T758 could cause charge–charge repulsion, leading to a reduction in binding affinity between pTβ2-CT and talin F3.

Furthermore, we examined the interactions of pTβ2-CT with talin F3 by employing mutations and peptide fragments of pTβ2-CT. Replacement of critical, interfacial aromatic residues W747A and F754A of pTβ2-CT resulted in a significant reduction in binding affinity to talin F3 (Supplementary Fig. S2 and Table 2). In order to dissect β2-CT/F3 binding, two overlapping peptide fragments, KS33 and pTDS20, of β2-CT were synthesized (Table 1) and examined for binding to talin F3. KS33 peptide fragment interacted with residues in the central β-sheet and the C-terminal helix of talin F3 (Fig. 4a). An apparent K_d was estimated to be 357 μM for KS33/talin F3 interactions (Fig. 4b and Table 2). By contrast, talin F3 showed no detectable interactions with pTDS20 peptide fragment (Supplementary Fig. S3). These data demonstrated that β2-CT and pTβ2-CT interacted with talin F3 domain, utilizing similar binding residues, however, with different affinity. The pTβ2-CT/talin interactions were characterized by low-affinity complex. Furthermore, analyses of talin binding with non-phosphorylated and phosphorylated β2 peptide fragments revealed that the non-phosphorylated N-terminal residues (KS33) of β2-CT contribute primarily to the binding.

Adaptor protein 14-3-3ζ, talin F3, and pTβ2-CT formed a ternary complex

NMR transverse relaxation (T_2) is a useful indicator of molecular weight and conformational exchange processes of proteins. We compared the backbone ^{15}N T_2 of talin F3 either in free solution or in the presence of pTβ2-CT or a mixture of both pTβ2-CT and 14-3-3ζ. The ^{15}N T_2 values of most of the residues of talin F3 in free solution showed uniform distribution with an average T_2 value of 50.84 ms (Supplementary Fig. S4). By contrast, residues of talin F3 exhibited a marked reduction of T_2 values (Supplementary Fig. S4), an estimated average of T_2 = 36 ms, in the presence of 14-3-3ζ and pTβ2-CT, presumably due to an increase in molecular weight and/or conformational exchange processes involving the ternary complex. Note that the ^{15}N T_2 values, an average of T_2 = ~46 ms, of talin F3 were not significantly affected in complex with pTβ2-CT (Supplementary Fig. S4).

We further examined the residues of talin F3 that interact with pTβ2-CT in the ternary complex. $^{15}N–^{1}H$ HSQC spectra of talin F3 were found to be invariant upon the addition of unlabeled 14-3-3ζ, suggesting a lack of detectable interactions (data not shown). $^{15}N–^{1}H$ HSQC spectra of talin F3, acquired in the presence of equimolar concentration of unlabeled 14-3-3ζ, showed changes in chemical shifts and intensity in the presence of increasing concentrations of pTβ2-CT. A number of residues of talin F3 showed differences in chemical shifts and

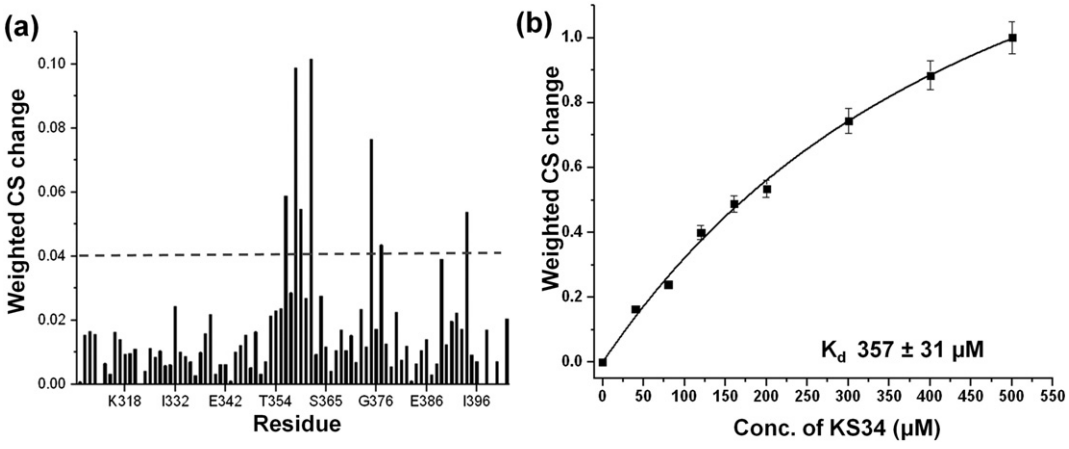


Fig. 4. Mapping talin F3 interactions with MP β2-CT peptide KS34. (a) Bar diagram showing combined CSP for ^{15}N and HN resonances of each residue of talin F3 upon binding to KS34 at F3:KS34 1:3 ratio. The dotted line marked average CSP. (b) Normalized chemical shift differences are plotted against the concentrations of KS34 for talin F3 to determine equilibrium dissociation constant (K_d) value.

line-broadening effects between F3/pTβ2-CT binary complex and F3/14-3-3ζ/pTβ2-CT ternary complex (Fig. 5a). A K_d of 213 μM, between F3/pTβ2-CT, in the presence of 14-3-3ζ was determined from the chemical shift change (Fig. 5b and Table 2). It was noted that a higher K_d value was obtained for F3/pTβ2-CT in the absence of 14-3-3ζ (Table 2). Weighted chemical shift changes (>0.04 ppm) and residues that showed peak broadening were mapped onto the 3D structure of talin F3 (Fig. 5c). Residues located in the β5 and β6 strands and adjacent loops with fewer residues in the C-terminal helix were perturbed in the ternary complex (Fig. 5c). The potential involvement of residues W747 and F754 of β2-CT in the talin F3/14-3-3ζ/pTβ2-CT ternary complex was further examined by individual $^{15}N–^{1}H$ HSQC titrations of ^{15}N-labeled talin F3 and unlabeled 14-3-3ζ with β2 W747A or F754A variants. In the ternary complex, mutant CTs demonstrated significantly higher K_d values compared to pTβ2-CT (Table 2 and Supplementary Fig. S5).

The binding interactions of the ternary complex of 14-3-3ζ/F3/pTβ2-CT were further determined by isothermal titration calorimetry (ITC), chemical cross-linking, and size-exclusion methods. In addition, ITC data were acquired for the binary complex of 14-3-3ζ, pTβ2-CT, and phosphorylated peptide fragment pTDS20. Representative ITC thermograms and binding parameters are shown (Fig. 6 and Table 3). Proteins/pTβ2-CT interactions were exothermic or enthalpy driven as indicated by negative heat exchange or negative ΔH values (Fig. 6, upper panels, and Table 3). Data also suggest that 14-3-3ζ interacted with either full-length pTβ2-CT or shorter CT fragment pTDS20 with similar K_d values of 4.9 μM or 11 μM, respectively (Fig. 6a and b, and Table 3). A recent study using ITC also estimated a K_d of 7.9 μM for the binding of 14-3-3ζ with pTβ2-CT [19]. Furthermore, our results corroborate well with previous reports that the C terminus or the MD region of phosphorylated β2-CT is largely responsible for the binding with 14-3-3ζ [14]. The binding affinity of the ternary complex was determined by injecting talin F3 into solutions of pre-formed binary complex of 14-3-3ζ and pTβ2-CT (Fig. 6c). Talin F3 interacted with pTβ2-CT/14-3-3ζ complex with an apparent K_d

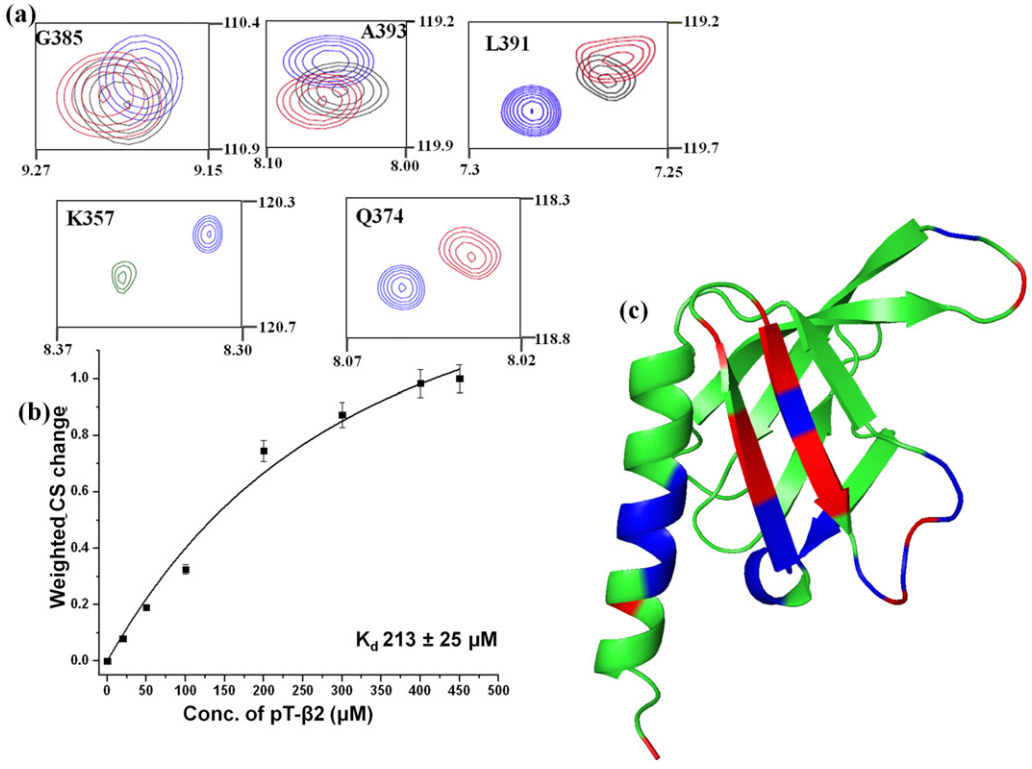


Fig. 5. Mapping talin F3 interactions with pTβ2-CT and 14-3-3ζ. (a) Overlay of the sections of $^{15}N–^{1}H$ HSQC spectra of representative residues of talin F3 alone (blue contour) in the presence of threefold excess of pTβ2-CT (green contour) and in the presence of both pTβ2 and 14-3-3ζ (in red contour; F3:14-3-3ζ:pTβ2 1:1:3). (b) Normalized chemical shift differences are plotted against the concentrations of pTβ2-CT for talin F3 to determine equilibrium dissociation constant (K_d) value. (c) A ribbon representation of the 3D structure of talin F3. Residues that exhibited above average CSPs and resonance broadening in the presence of β2-CT and 14-3-3ζ are shown as blue and red, respectively.

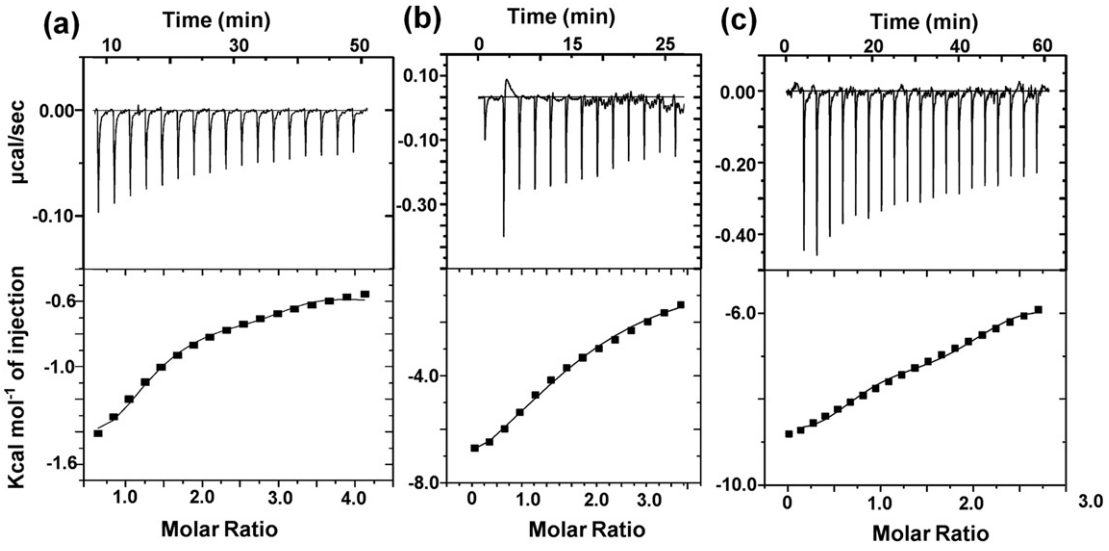


Fig. 6. Thermodynamic characterization of interactions among pTβ2-CT, talin F3, and 14-3-3ζ in ternary complex by ITC. (a) ITC titrations of binding of the full-length pTβ2-CT with 14-3-3ζ. (b) ITC titrations of binding of the Thr phosphorylated peptide fragment pTDS20 of pTβ2-CT (Table 1) with 14-3-3ζ. In both titrations, aliquots of fixed amount of phosphorylated β2-CT peptides were injected into sample cells containing 14-3-3ζ. (c) ITC titrations of binding of the talin F3 with the pre-formed complex of full-length pTβ2-CT and 14-3-3ζ. Aliquots of fixed amount of F3 samples were injected into sample cells containing equimolar concentrations of pTβ2-CT and14-3-3ζ. The top panels of the ITC thermograms show heat exchange of binding, whereas the heat of reaction as a function of molar ratios is shown at the bottom panels.

of 161.8 μM (Table 3). A comparable K_d value of 213 μM was estimated from ^{15}N–^{1}H HSQC titration experiments of talin F3 (Table 2). Therefore, talin F3 appeared to interact with the complex of pTβ2-CT/14-3-3ζ with relatively higher affinity in comparison to the binary complex of talin F3/pTβ2-CT. The determination of binding affinity between pTβ2-CT and talin F3 by ITC was unsuccessful, presumably due to the weak affinity of interactions that resulted in non-saturable binding thermograms. It has been postulated that the interactions of integrin CTs with effector proteins may be modulated in membrane bilayer [2,16]. Notably, talin binding affinity of β3-CT or CT/CT interactions appeared to be enhanced in model membrane mimic systems [20,21]. Therefore, we also examined the binding of 14-3-3ζ with pTβ2-CT and of Dok1 with di-phosphorylated pSpTβ2-CT (vide infra) (Table 1) in membrane mimic solutions containing dodecylphosphocholine by ITC (Supplementary Fig. S6). Our results showed that proteins/CTs binding affinities were significantly diminished in membrane mimic solutions. 14-3-3ζ and Dok1 bind to phosphorylated CTs with K_d values of 649 μM and 3.5 mM, respectively (Supplementary Fig. S6).

Ternary complexes of 14-3-3ζ, talin F3, and pTβ2-CT proteins were further examined by glutaraldehyde-mediated chemical cross-linking and size-exclusion chromatography. Protein components were mixed in buffer solutions of 2% glutaraldehyde, and samples were electrophoresed in SDS-PAGE gel at different time points (Supplementary Fig. S7). Protein band corresponding to the molecular weight of the ternary complex could be detected in the SDS-PAGE gel (Supplementary Fig. S7). In size-exclusion chromatography experiments, the ternary complex of 14-3-3ζ/F3/pTβ2-CT can be co-eluted and observed in SDS-PAGE (Supplementary Fig. S8).

Exclusion of Dok1 from β2-CT in the presence of 14-3-3ζ and talin F3

We probed changes in ^{31}P NMR signal of phosphorylated β2-CTs, that is, monophosphorylated pTβ2-CT and di-phosphorylated pSpTβ2-CT (Table

Table 3. ITC interaction analyses of the binding of pTβ2-CT, 14-3-3ζ, and talin F3

Cell Conc. (μM)		Syringe Conc. (μM)		K_d	Δ*H* (Kcal/mol)	*T*Δ*S* (Kcal/mol)	Δ*G* (Kcal/mol)
14-3-3ζ	25	pTβ2	580	4.9 ± 1.2	−13.22	−5.97	−7.25
14-3-3ζ	10	pTβ2 MD	220	11.03 ± 1.2	−10.29	−11.7	6.54
pTβ2:14-3-3ζ	25	F3	800	161.8 ± 31.2	−17.94	−12.75	−5.18

1) in complex with 14-3-3ζ, talin F3, and Dok1 proteins. Figure 7a shows a set of ^{31}P NMR spectra of pTβ2-CT in the absence (lower panel) and in the presence of talin F3, 14-3-3ζ, or 14-3-3ζ/F3 combined. In free solution, pTβ2-CT yielded a sharp ^{31}P NMR signal characteristic of unstructured protein undergoing fast motion. ^{31}P NMR spectrum of pTβ2-CT in complex with talin F3 showed a discernable change in line width and a slight change in chemical shift compared to the ^{31}P spectrum of free pTβ2-CT, thus inferring certain interaction, but phosphorylated Thr is not the site of interaction. By contrast, dramatic changes, in terms of chemical shift and line width, in ^{31}P NMR spectrum of pTβ2-CT were observed upon inclusion of 14-3-3ζ. The downfield shift of ^{31}P signal of pTβ2-CT in the presence of 14-3-3ζ would indicate direct interactions of the phosphate group of residue pThr758 with binding residues of 14-3-3ζ. ^{31}P NMR spectrum of pTβ2-CT in the presence of both 14-3-3ζ and talin F3 revealed further increased line width, with certain change of chemical shift, compared to the binary pTβ2-CT complexes of F3 and 14-3-3ζ (Fig. 7a). ^{31}P NMR of pTβ2-CT therefore also revealed that 14-3-3ζ/pTβ2-CT complex can recruit talin F3 in a ternary complex.

Dok1 protein is a negative regulator of integrin, whereby binding of the PTB domain of Dok1 to the phosphorylated β-CTs displaces talin from integrin [7,22-24]. Therefore, we investigated the effect of the binding of 14-3-3ζ and Dok1 proteins to phosphorylated β2-CT. The PTB domain of Dok1 binds to β2-CT with high affinity upon phosphorylation of residue Ser756 [8]. We made use of di-phosphorylated pSpTβ2-CT for 14-3-3ζ and Dok1 interactions. Figure 7b shows ^{31}P NMR spectra of pSpTβ2-CT in free solution (lower panel), in complex with 14-3-3ζ (middle panel) and in the presence of 14-3-3ζ and Dok1 (upper panel). Both of the ^{31}P resonances of pSpTβ2-CT showed large chemical shift changes in the presence of 14-3-3ζ (Fig. 7b). However, there were no noticeable changes in ^{31}P NMR signals upon further inclusion of equimolar concentration of Dok1 (Fig. 7b). Therefore, ^{31}P NMR studies of the pSpTβ2-CT demonstrated that Dok1 was unable to interact with the di-phosphorylated pSpTβ2-CT in the presence of 14-3-3ζ. Taken together, these results suggest that while talin F3 and 14-3-3ζ could form a ternary complex with β2-CT, the negative regulator Dok1 was unable to bind to β2-CT in the presence of 14-3-3ζ.

Structure model of the ternary complex

At present, we are unable to determine atomic-resolution structure of the entire ternary complex of 14-3-3ζ/talin F3/pTβ2-CT. However, based on data from existing binary complexes, we modeled the ternary complex of pTβ2-CT, talin F3, and 14-3-3ζ in order to discern potential intermolecular contacts (see Materials and Methods). The overall topology of the ternary complex and molecular interactions are shown (Fig. 8a). The ternary complex of 14-3-3 ζ/pTβ2/talin F3 could be modular in nature, whereby most of the intermolecular interactions observed in the binary complexes of 14-3-3ζ/pTβ2 peptide fragment and talin F3/β2-CT are largely conserved. The MD region of pTβ2-CT carrying residue pT758 occupies the binding pocket of 14-3-3ζ, whereas the MP helix of the CT is engaged in interactions with talin F3 domain. In the docked structure, the phosphate group of pT758 is in close proximity to the guanidinium sidechain of residues R127, R56, and R60 (Fig. 8b), akin to the structure of 14-3-3ζ/pTβ2-CT complex [14]. The MP helix of pTβ2-CT maintained its interactions with the β-sheet region of talin F3 through potential salt bridges involving residue D731 of β2-CT and residues K322 and K324 of talin F3 (Fig. 8c). Hydrophobic packing interactions could form between the aromatic residues W747 of pTβ2-CT and the residues Y377 and W351 of F3 domain (Fig. 8d). The NPLF motif of pTβ2-CT could serve as a potential hinge between the talin F3 and 14-3-3ζ with fewer intermolecular contacts.

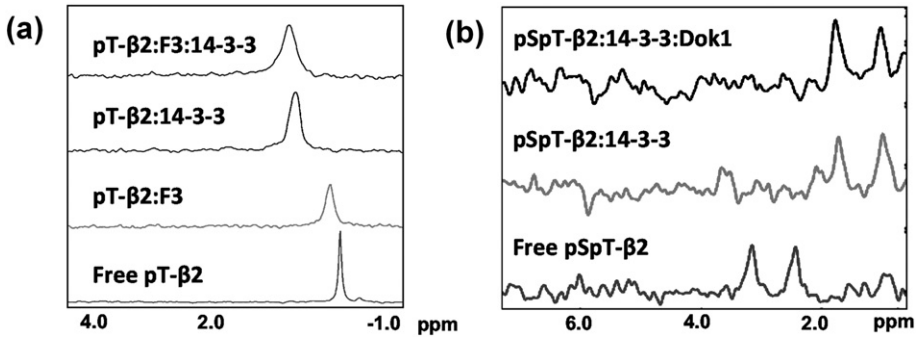


Fig. 7. Interactions of pTβ2-CT and pSpTβ2-CT with 14-3-3ζ, Dok1, and talin F3. (a) ^{31}P NMR spectra of pTβ2-CT in free solution, in the presence of talin F3 (pTβ2:F3, 1:0.5), 14-3-3ζ (pTβ2:14-3-3ζ, 1:0.5), and talin F3 and 14-3-3ζ (pTβ2:F3:14-3-3ζ, 1:0.5:0.5). (b) ^{31}P NMR spectra of pSTβ2-CT in free solution, in the presence of 14-3-3ζ (SpTβ2:14-3-3ζ, 1:1) and with Dok1 and 14-3-3ζ (pTβ2:Dok1:14-3-3ζ, 1:1:1).

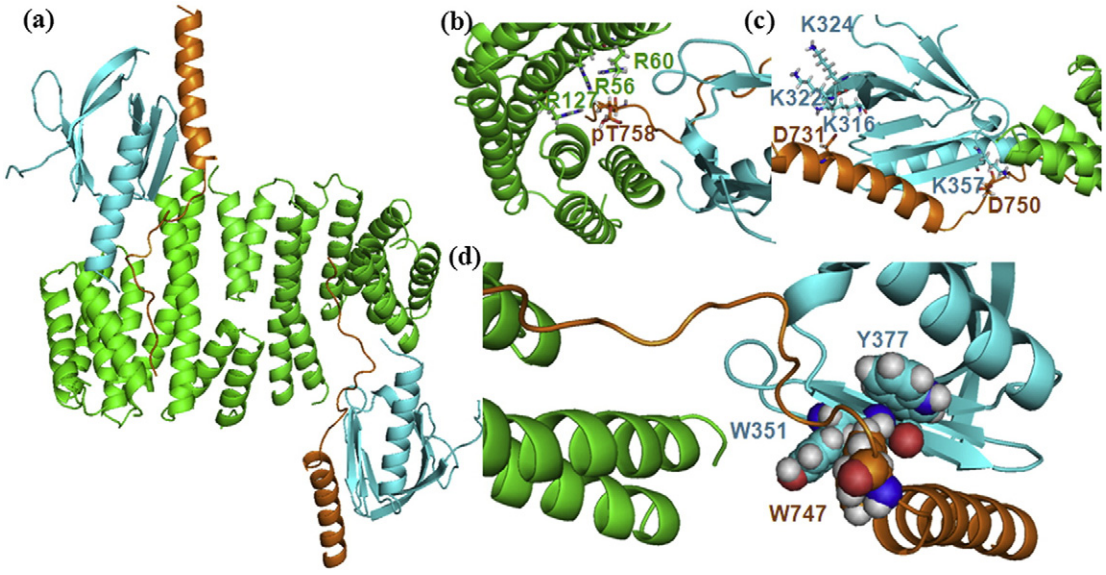


Fig. 8. Docked structure of the ternary complex of talin F3, 14-3-3ζ, and pTβ2-CT. (a) A ribbon representation of the topology of the ternary complex; dimeric 14-3-3ζ in green, talin F3 in cyan, and pTβ2-CT in light red. (b) Ionic interactions of residue pT758 of pTβ2-CT with cationic residues R127, R56, and R60 of 14-3-3ζ at the canonical phosphorylated peptide binding pocket. (c) Potential ionic and non-polar packing interactions of pTβ2 with talin F3, residue D731 of the MP helix, and residue D749 of β2-CT are in close proximity to the cationic residues of talin F3. (d) Potential aromatic packing interactions may involve residue W747 of pTβ2-CT and residues Y377 and W351 of talin F3.

Discussion

The interaction between the integrin β-CT and the F3 subdomain of talin plays an important role in integrin activation [2,25–28]. This association brings about the separation of the integrin α and β-CTs that leads to allosteric conformational changes in the integrin ectodomain that are necessary for binding ligands (1–3, 25). Based on x-ray crystallography, the atomic-resolution structure of talin-2 F2F3 domain in complex with integrin β1D-CT has been reported [16]. Although it is well accepted that talin binds integrin β-CT, there are clear differences in the binding affinities of talin with different integrin β-CTs. NMR interaction studies reported low-affinity complexes of talin/integrin β3-CT with a K_d value of ~273 μM and of talin/integrin β1A-CT with a K_d value of ~490 μM [29]. However, talin-2/integrin β1D-CT and talin-1/integrin β1D-CT complexes showed high-affinity interactions with a K_d value of ~36 μM and 95 μM, respectively (16, 29). These data suggest that subtle differences in the sequences of integrin β-CTs could affect their interactions with talin and other binding partners (Supplementary Fig. S9). As compared with other integrin β-CTs, β2-CT contains a few distinct motifs. These include a non-phosphorylatable NxxF motif instead of the highly conserved NxxY motif found in other β-CTs. It also contains a phosphorylatable TTT motif, which may give rise to differential interactions with talin and other effector proteins. Our results showed that talin F3 interacted with integrin β2-CT with low binding affinity K_d value of ~244 μM that is comparable to that between talin F3 and integrin CT β3 or β1A. However, it is difficult to determine the atomic structure of the talin F3/integrin β2-CT complex because of their transient interactions and resonance broadening. Indeed, similar challenges were encountered in the structural characterization of talin F3/integrin β3-CT complex [17]. Instead, a hybrid peptide or a peptide fragment of integrin β3-CT covalently linked to talin F3/F2 was used for the structure determination [17,30]. Nevertheless, we were able to map the binding of integrin β2-CT onto talin F3 that includes the C-terminal long helix, β-strands S5 and S4, an adjoining loop and β-strand 7, and a loop between S1 and S2 (Fig. 1d) based on above average chemical shift changes and resonance broadening. These structural elements of talin F3 were also found to be involved in the complex formation with integrin β3-CT. The docked structure of talin F3 and integrin β2-CT suggests potential intermolecular interactions within the complex (Fig. 2b). The interactions between talin F3 and the N-terminal MP part of integrin β2-CT are found to be conserved with that of the talin F3/chimeric integrin β3-CT and the talin F3/integrin β1D-CT complexes [16,17]. However, comparison of packing interactions involving talin F3 and the MD region of the integrin β-CTs remains challenging due to sequence variations among the β-CTs. Our ^{15}N–^{1}H HSQC binding data showed interactions between talin F3 and the MP region of β2 peptide fragment (KS33), whereas no

detectable binding was observed for the phosphorylated MD peptide (pTDS20; Table 2). These data suggest that in addition to the MP region, the MD region of the integrin β-CTs may modulate talin/β-CTs complex formation. Phosphorylation of integrin CTs, both α and β, plays critical roles in regulating their interactions with effector proteins [2,21,31,32]. Phosphorylation of residue Y^{747} in NPxY in integrin β3-CT promotes the binding of Dok1, a negative regulator of integrin activation [7,22,23]. Talin/integrin β3-CT interactions have been shown to be significantly reduced upon phosphorylation of Y^{747} [7,22,23]. Given that integrin β2-CT contains two non-phosphorylatable NPxF motifs instead of the NPxY motifs (Supplementary Fig. S9), the above mechanism of regulation with respect to talin interaction is unlikely. However, integrin β2-CT contains phosphorylatable Ser and Thr residues that could be involved in integrin activation and regulation [8]. Indeed, we have shown that phosphorylation of integrin β2-CT residue S756 that resides between the $NPxF^{754}$ and the $T^{758}TT$ motifs promotes Dok1 binding [8]. Phosphorylation of residue T758 in the TTT motif of integrin β2-CT and the corresponding residue in integrin β3 and β7 CTs were reported to be involved in integrin activation [14]. pT758 of integrin β2 facilitated the binding of 14-3-3ζ but inhibited the binding of negative regulator filamin to β2-CT [14,31-35]. 14-3-3ζ also binds to phosphorylated α4 CT of integrin [19]; however, its binding to phosphorylated α-CTs of β2 integrins has yet to be reported. We therefore examined the effect of pT758 on the interactions between integrin β2-CT and talin F3. Interestingly, talin F3 interacted with T758-phosphorylated β2-CT (pT758β2-CT) with twofold lower affinity as compared to β2-CT (Table 2). Since pT758β2-CT recruits 14-3-3ζ, we performed in-depth analyses of the interactions among pT758β2-CT, talin F3, and 14-3-3ζ so as to gain insights into complex formation. We demonstrated that pT758β2-CT forms a ternary complex with talin F3 and 14-3-3ζ. Remarkably, in the ternary complex, pT758β2-CT/talin F3 interacted with a lower K_d value. However, the interaction affinity between pT758β2-CT and 14-3-3ζ remained invariant as compared to that of the binary complexes (Table 2). Interaction analyses using integrin β2-CT peptide fragments further mapped the possible interaction sites of talin F3 and 14-3-3ζ in the ternary complex. It should be noted that in the ternary complex, talin F3 and 14-3-3ζ did not show any apparent interactions. Talin F3 interacts with the MP region of integrin β2-CT, whereas 14-3-3ζ interacts with the $pT^{758}TT$ motif and the MD region of integrin β2-CT (Fig. 8). Interactions of the talin F3 with the MP helix of integrin β-CTs are known to be crucial for talin-mediated activation of integrins [2,4,5]. Our study also demonstrated that W747 in the MP region of integrin β2 is required for talin F3 interaction in both the binary complex and the ternary complex with 14-3-3ζ. Residue W747 displays multiple packing interactions with talin F3 that could be important in the complex formation. These data are in line with a previous study that showed the interactions between talin and integrin β3 and between β1A and β1D CTs involving this conserved Trp [29].

A recent study demonstrated the possibility of a ternary complex of filamin or domain FLA-IgN21with integrin αIIb and β3 CTs such that filamin interacts with both CTs while maintaining their interactions [36]. Notably, the MP helix of β3-CT delineated the packing with FLA-IgN21, causing a folding back of the β-CT. Furthermore, the Dok1 binding site involving the NPxY motif of β3 CT in the ternary complex is largely exposed. Based on our findings and that of others [36–38], we propose a sequential model of β2 integrin inside-out activation followed by outside-in signaling (Fig. 9). In the resting state, the integrin β2-CT is engaged with the negative regulators Dok1 and filamin (Fig. 9). It should be noted that Dok1 is involved in both inside-out [8] and outside-in [39] signaling of integrins. Upon cellular activation, the following series of inside-out β2 integrin activation events could occur: (i) kindlin-3 docks onto the distal NPKF motif in the β2-CT. Kindlin-3 could recruit migfilin that displaces filamin from the β2-CT [40–42]; (ii) β2-CT pS756 is dephosphorylated and it leads to the release of Dok1, thereby allowing the talin head domain to associate with the β2-CT involving the NPLF motif; (iii) concomitantly, β2-CT pT758 is phosphorylated, which promotes 14-3-3ζ binding; and (iv) the binding of 14-3-3ζ to the β2-CT leads to the repositioning of talin head domain, facilitating ternary complex formation. These events lead to the activation of β2 integrins, allowing them to bind ligands. Given that talin interacts with the actin cytoskeleton and that 14-3-3ζ has the potential to dimerize, such ternary complex formation could have an important role in integrin clustering, which is required for integrin outside-in signaling. In conclusion, our study provides evidence of ternary complex formation of 14-3-3ζ, pTβ2-CT, and talin F3. We have performed co-immunoprecipitation experiment to check for ternary complex using 293T cells transfected with integrin αLβ2, talin head domain, and 14-3-3ζ, but we were unsuccessful (data not shown). Future cell-based experiments using different approaches will be necessary to validate the *in vitro* data. Notwithstanding, our data provide an important first step toward the understanding of sequential events leading to β2 integrin inside-out activation and outside-in signaling.

Materials and Methods

Protein expression and purification

N-terminal six His-tag talin F3 domain (G309-S405), Dok1 PTB domain (Q154-G256), and 14-3-3ζ

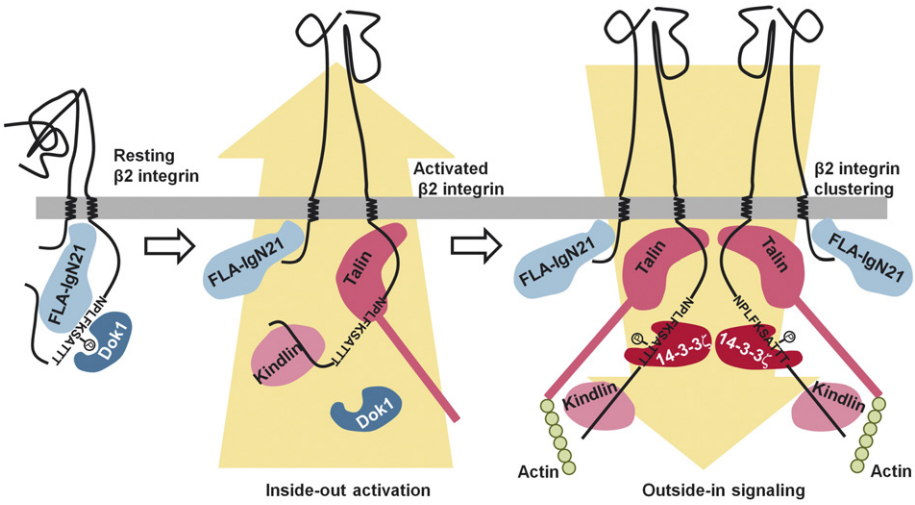


Fig. 9. A proposed model of β2 integrin activation that involves complex formation with talin and 14-3-3ζ. In its resting state, β2 integrin adopts a bent conformation with clasped transmembrane domains and CTs. This is maintained by filamin that binds to two regions within β2-CT and the MP region in the α-CT. In the resting β2 integrin, Ser756 could be phosphorylated, which promotes Dok1 binding. Upon cellular activation, kindlin-3 is recruited to the NPKF motif of the β2-CT. Kindlin-3 binds to migfilin that could displace filamin from its β2-CT binding sites, but filamin could still retain its interaction with the α-CT. Concomitantly, pSer756 could be dephosphorylated by a yet unknown mechanism. This leads to the dissociation of Dok1 from its β2-CT binding site. The release of both filamin and Dok1 from the β2-CT allows talin binding. This disrupts the salt bridge interaction between the β2 integrin CTs, leading to the separation of the CTs and transmembrane domains. As a consequence, the β2 integrin undergoes global conformational changes from a bent to an extended conformation, which is a hallmark of integrin inside-out activation. At this stage, Thr758 in the β2-CT could be phosphorylated, and it promotes 14-3-3ζ binding. 14-3-3 family of proteins is known to form homodimers. Hence, a 14-3-3ζ monomer on one β2-CT could homodimerize with another 14-3-3ζ monomer on another β2-CT, leading to β2 integrin clustering. Given that talin rod region binds the actin, the β2 integrin cluster is further stabilized by talin–filamentous actin interactions. The clustering of β2 integrins and their linkages to the actin cytoskeleton not only increases the overall avidity of ligand binding but also induces outside-in signaling.

(M1-S230) were generated by sub-cloning respective synthetic genes with *Escherichia coli*-optimized codons into the pET14b vector. Residue Cys 336 of F3 was mutated to Ser to avoid undesirable disulfide bond formation. Transformed *E. coli* BL21(DE3) cells were grown at 37 °C either in LB or in M9 medium containing [^{15}N] ammonium chloride and [^{13}C] D-glucose (Cambridge Isotope Laboratories). Protein expression was induced by adding IPTG (0.5 mM) to the cell culture (OD_{600} = ~0.6–0.7), followed by incubation for 10–12 h at 18 °C. Proteins were purified as previously reported [8]. Cells were centrifuged and resuspended in buffer A [50 mM sodium phosphate buffer and 300 mM NaCl (pH 8.0)], followed by affinity purification on a Nickel-NTA column (GE). His-tagged proteins were eluted in buffer B [50 mM sodium phosphate buffer, 500 mM imidazole, and 300 mM NaCl (pH 8.0)] using AKTA FPLC UPC-900 system (GE Healthcare UK Ltd., England) and were exchanged against buffer C [20 mM sodium phosphate buffer and 50 mM NaCl (pH 6.0)]. His-tagged proteins were then subjected to size-exclusion chromatography in buffer C on a Hiload Superdex 75 16/26 GL preparative column at a flow rate of 0.3 ml/min. Eluted proteins were monitored by absorbance at λ = 276 nm. The β2-CT (K724-S769) was sub-cloned into the pET-31b(+) vector to generate fusion proteins containing N-terminal ketosteroid isomerase (KSI) as previously described [43]. The same protocol was followed for the purification of β2-CT fusion protein, except for the buffer A and B that contained 8 M urea. The eluted proteins were dialyzed against water to remove urea that resulted in the precipitation of fusion protein. Fusion protein was incubated in 90% formic acid and purged with N_2 gas for 22 h in the dark to cleave the Asp–Pro peptide bond between the ketosteroid isomerase and β2-CT. Formic acid was neutralized with sodium hydroxide using a rotary evaporator, leaving a film of precipitate. The precipitate was dissolved in water and further purified using HPLC. The identities of the cleaved peptides were verified by mass spectrometry.

Synthetic peptides

Synthetic β2-CT and phosphorylated β2-CT and β2 peptide fragments (Table 1) were purchased from GLBioChem™, Shanghai, China and were further purified using HPLC (Waters™ 2489). Molecular weight of the peptides was confirmed by mass spectrometry.

NMR spectroscopy

All NMR experiments were performed on a Bruker DRX 600 MHz spectrometer equipped with an actively shielded cryoprobe. ^{31}P NMR spectra were recorded at Bruker 400 MHz spectrometer. NMR data were processed using NMRPIPE or Topspin 3.0 and analyzed by Sparky (T.D. Goddard and D.G. Kneller, University of California, San Francisco). The chemical shifts were directly or indirectly referenced to 2,2-dimethyl-2-silapentane-5-sulfonate. ^{15}N–^{1}H HSQC spectra for ^{15}N-labeled talin F3 and β2-CT were acquired at a concentration of 0.1 mM in buffer C [20 mM sodium phosphate buffer and 50 mM NaCl (pH 6.0)]. ^{15}N–^{1}H HSQC resonance assignments of talin F3 were achieved by 3D experiments (HNCACB, CBCA(CO)NH) of ^{15}N/^{13}C-labeled talin F3 (0.3 mM) samples in buffer C. For NMR titration, ^{15}N–^{1}H HSQC spectra of protein samples were recorded after 10 min of equilibration with sequential addition of binding partners. Stock solutions of 3.8 mM, 5.1 mM, 4.2 mM, and 3.1 mM of β2-CT, pTβ2-CT, KS33, and pTDS20, respectively, were used to titrate against 0.1 mM ^{15}N-labeled talin F3 at different molar ratios (1:0.4, 1:0.8, 1:0.1.2, 1:1.6, 1:2, 1:3, 1:4, and 1:5). ^{15}N–^{1}H HSQC titrations were carried out with pTβ2-CT and β2 peptide fragments in solutions containing equimolar mixture (0.1 mM) of ^{15}N-labeled talin F3 and unlabeled 14-3-3ζ. ^{15}N–^{1}H HSQC spectra of ^{15}N-labeled β2-CT were acquired in the presence of unlabeled talin F3 (0.7 mM stock) at different molar ratios (1:0.5, 1:1, 1:1.5, 1:2, 1:2.5, and 1:3). Ligand-induced chemical shift changes in ^{15}N and HN resonances were determined using the following equation, which is designated as CSP: $\Delta(H,N) = [\{(\Delta H)(WH)\}^2 + \{(\Delta N)(WN)\}^2]^{1/2}$, where WH and WN are weighting factors for ^{1}H and ^{15}N chemical shifts, respectively (WH = 1; WN = 0.154), and ΔH and ΔN are the chemical shift difference for HN and ^{15}N, respectively. The K_d values were calculated from the depletion model for ligand binding following the equation: $\Delta(H,N) = \Delta(H,N)_{max}[\{[L] + [U] + K_d\} - [\{[L] + [U] + K_d\}^2 - 4[L][U]]^{1/2}] \div 2$ [L], where $\Delta(H,N)$ and $\Delta(H,N)_{max}$ are the weighted chemical shift and weighted chemical shift at saturation, respectively; K_d represents the dissociation constant; and [L] and [U] are the concentrations of protein and unlabeled peptides, respectively. Well-resolved ^{15}N–^{1}H HSQC peaks with significant chemical shift changes were used to fit the above equation using OriginPro 9.0 in order to determine the K_d values. The dissociation constant is presented as K_d ± S.E. (standard error). The error bar indicates the standard deviation for each titration point.

Relaxation measurement

The T_2 rates of ^{15}N nuclei of backbone of talin F3 were determined by collecting a series of ^{15}N–^{1}H HSQC spectra of 0.1 mM talin F3 alone and talin F3 + pTβ2-CT (1:3) talin F3 + 14-3-3ζ + pTβ2-CT (1:1:3) with sensitivity enhancement in a Bruker DRX 600 MHz spectrometer at 298 K temperature. T_2 measurements were acquired with delays of 14.4, 28.8, 43.2, 57.6, 72.0, 86.4, 100.8, 115.2, 129.6, 144.0, and 158.4 ms and were repeated twice for all the experimental conditions. T_2 values were estimated by fitting the cross-peak intensities to a mono-exponential function as in $I = A^*\exp(R^*t)$, where I, A, R, and t represent signal intensity, constant, relaxation value, and time point, respectively.

^{31}P NMR experiments

^{31}P NMR spectra of pTβ2-CT were recorded on a Bruker DRX 400 spectrometer with dual channel RT probe at 298 K and at 0.2 mM peptide concentrations. Data acquisition and processing were performed with the Topspin software (BRUKER) suite. ^{31}P NMR spectra of pTβ2-CT in a buffer containing 20 mM Tris and 50 mM NaCl (pH 6.0) were recorded with talin F3 and 14-3-3ζ, 0.1 mM each. Using the same buffer condition, ^{31}P NMR spectra of 100 μM pSApTβ2-CT were acquired with equimolar concentrations of Dok1 PTB domain and 14-3-3ζ.

ITC

All samples were prepared in 20 mM sodium phosphate and 50 mM NaCl (pH 6.5). ITCs were performed in a VP-ITC200 instrument at 298 K. For 14-3-3ζ/phosphorylated CTs binding, fixed amounts of either pTβ2-CT or pTDS20 peptide were injected into cell (200 μl) containing 14-3-3ζ. For the ternary complex, fixed concentrations of F3 were injected into cell (200 μl) containing equimolar mixture of 14-3-3ζ and pTβ2-CT. Interactions of 14-3-3ζ and Dok1 with pTβ2-CT and pSpTβ2-CT, respectively, were carried out in 20 mM sodium phosphate and 50 mM NaCl (pH 6.5) containing 10 mM dodecylphosphocholine. ITC experiments in dodecylphosphocholine were performed with either 25 μM 14-3-3ζ (in cell) or 20 μM Dok1(in cell). pTβ2-CT (690 μM) and pSpTβ2-CT (290 μM) were kept in syringe. Typically, the first injection of 0.2 μl was followed by 19 injections of 2 μl, with 150-s time delay between two injections, and samples stirred at a speed of 900 rpm. Taking care of the heat of dilution, we performed a blank titration by injecting proteins into buffer. All raw data were processed using MicroCal Origin software.

Chemical cross-linking

Glutaraldehyde-mediated protein cross-linking experiments were carried out with reaction mixtures containing 14-3-3ζ:talin F3:pTβ2-CT at 1:1:3 M ratios and 14-3-3ζ:pTβ2-CT at 1:3 M ratios in 20 mM sodium

phosphate and 50 mM NaCl (pH 8.0) with a total volume of 100 μl, in the presence of 2 μl of 2% freshly prepared solution of glutaraldehyde at 37 °C. Samples were collected at different time intervals, and reactions were quenched by the addition of 1.5 M Tris–HCl (pH 8.0). Cross-linking was observed by conducting electrophoresis in 16% SDS-polyacrylamide gel.

Size-exclusion chromatography

A Hiload Superdex 75 16/26 GL preparative column using AKTA FPLC UPC-900 system (GE Healthcare UK Ltd., England) was employed for size-exclusion chromatography. A solution of 500 μl of 14-3-3ζ:talin F3:pTβ2-CT in 1:1:3 ratio was injected and eluted with 20 mM sodium phosphate buffer and 50 mM NaCl (pH 6.0) at a flow rate of 0.30 ml/min. Formation of ternary complex was determined by 16% SDS-polyacrylamide gel.

Docking of talin F3 with pTβ2-CT and 14-3-3ζ

Structural models of β2-CT and pTβ2 were constructed based on the 3D structures of β1D/talin 2 [14] and pTβ2 peptide/14-3-3ζ [12] complexes using InsightII (Accelrys Inc.). Docked models of binary β2-CT/talin F3 (PDB: 2h7d) and ternary pTβ2-CT/talin F3/14-3-3ζ (PDB: 2v7d) complexes were derived using ZDOCK program† based on chemical shift changes and cross-peak boarding. The model structures were validated using ADIT Validation Server from the Protein Data Bank.

Acknowledgment

This work was supported by a grant (ARC18/13) from the Ministry of Education (MOE), Singapore.

Appendix A. Supplementary Data

Supplementary data to this article can be found online at http://dx.doi.org/10.1016/j.jmb.2016.08.014.

Received 11 May 2016;
Received in revised form 11 August 2016;
Accepted 15 August 2016
Available online 18 August 2016

Keywords:
β2 integrins;
NMR;
protein–protein interaction;
talin;
14-3-3

†http://zdock.umassmed.edu

Abbreviations used:
CT, cytoplasmic tail; MP, membrane-proximal; PTB, phosphotyrosine binding; MD, membrane-distal; CSP, chemical shift perturbation; ITC, isothermal titration calorimetry; pT758β2-CT, T758-phosphorylated β2-CT.

References

[1] R.O. Hynes, Integrins: bidirectional, allosteric signaling machines, Cell 110 (2002) 673–687.
[2] N.J. Anthis, I.D. Campbell, The tail of integrin activation, Trends Biochem. Sci. 36 (2001) 191–198.
[3] S.M. Tan, The leucocyte β2 (CD18) integrins: the structure, functional regulation and signalling properties, Biosci. Rep. 32 (2012) 241–269.
[4] D.R. Critchley, A.R. Gingras, Talin at a glance, J. Cell Sci. 121 (2008) 1345–1347.
[5] S. Tadokoro, S.J. Shattil, K. Eto, V. Tai, R.C. Liddington, J.M. de Pereda, M.H. Ginsberg, D.A. Calderwood, Talin binding to integrin β tails: a final common step in integrin activation, Science 302 (2003) 103–106.
[6] D.A. Calderwood, B. Yan, J.M. de Pereda, B.G. Alvarez, Y. Fujioka, R.C. Liddington, M.H. Ginsberg, The phosphotyrosine binding-like domain of talin activates integrins, J. Biol. Chem. 277 (2002) 21,749–21,758.
[7] C.L. Oxley, N.J. Anthis, E.D. Lowe, I. Vakonakis, I.D. Campbell, K.L. Wegener, An integrin phosphorylation switch: the effect of beta3 integrin tail phosphorylation on Dok1 and talin binding, J. Biol. Chem. 283 (2008) 5420–5426.
[8] S. Gupta, J.C. Chit, C. Feng, A. Bhunia, S.M. Tan, S. Bhattacharjya, An alternative phosphorylation switch in integrin β2 (CD18) tail for Dok1 binding, Sci. Rep. 5 (2015) 11,630.
[9] H. Fu, R.R. Subramanian, S.C. Masters, 14-3-3 proteins: structure, function, and regulation, Annu. Rev. Pharmacol. Toxicol. 40 (2000) 617–647.
[10] M. Uhart, A.A. Iglesias, Bustos DM structurally constrained residues outside the binding motif are essential in the interaction of 14-3-3 and phosphorylated partner, J. Mol. Biol. 406 (2011) 552–557.
[11] M. Chen, T. Liu, L. Xu, X. Gao, X. Liu, C. Wang, Q. He, G. Zhang, L. Liu, Direct interaction of 14-3-3ζ with ezrin promotes cell migration by regulating the formation of membrane ruffle, J. Mol. Biol. 426 (2014) 3118–3133.
[12] S. Fagerholm, N. Morrice, C.G. Gahmberg, P. Cohen, Phosphorylation of the cytoplasmic domain of the integrin CD18 chain by protein kinase C isoforms in leukocytes, J. Biol. Chem. 277 (2002) 1728–1738.
[13] S.M. Nurmi, C.G. Gahmberg, S.C. Fagerholm, 14-3-3 proteins bind both filamin and alphaLbeta2 integrin in activated T cells, Ann. N. Y. Acad. Sci. 1090 (2006) 318–325.
[14] H. Takala, E. Nurminen, S.M. Nurmi, M. Aatonen, T. Strandin, M. Takatalo, T. Kiema, C.G. Gahmberg, J. Ylanne, S.C. Fagerholm, Beta2 integrin phosphorylation on Thr758 acts as a molecular switch to regulate 14-3-3 and filamin binding, Blood 112 (2008) 1853–1862.
[15] T. Kiema, Y. Lad, P. Jiang, C.L. Oxley, M. Baldassarre, K.L. Wegener, I.D. Campbell, J. Ylanne, D.A. Calderwood, The

molecular basis of filamin binding to integrins and competition with talin, Mol. Cell 21 (2006) 337–347.
[16] N.J. Anthis, K.L. Wegener, F. Ye, C. Kim, B.T. Goult, E.D. Lowe, I. Vakonakis, N. Bate, D.R. Critchley, M.H. Ginsberg, I.D. Campbell, The structure of an integrin/talin complex reveals the basis of inside-out signal transduction, EMBO J. 28 (2009) 3623–3632.
[17] K.L. Wegener, A.W. Partridge, J. Han, A.R. Pickford, R.C. Liddington, M.H. Ginsberg, I.D. Campbell, Structural basis of integrin activation by talin, Cell 128 (2007) 171–182.
[18] K. Bledzka, K. Bialkowska, H. Nie, J. Qin, T. Byzova, C. Wu, E.F. Plow, Y.Q. Ma, Tyrosine phosphorylation of integrin beta3 regulates kindlin-2 binding and integrin activation, J. Biol. Chem. 285 (2010) 30,370–30,374.
[19] R. Bonet, I. Vakonakis, I.D. Campbell, Characterization of 14-3-3-ζ interactions with integrin tails, J. Mol. Biol. 425 (2013) 3060–3072.
[20] D.T. Moore, P. Nygren, H. Jo, K. Boesze-Battaglia, B. JS, W.F. DeGrado, Affinity of talin-1 for the β3-integrin cytosolic domain is modulated by its phospholipid bilayer environment, Proc. Natl. Acad. Sci. U. S. A. 109 (2012) 15,825–15,834.
[21] G.L. Chua, X.Y. Tang, M. Amalraj, S.M. Tan, S. Bhattacharjya, Structures and interaction analyses of integrin αMβ2 cytoplasmic tails, J. Biol. Chem. 286 (2011) 43,842–43,854.
[22] D.A. Calderwood, Y. Fujioka, J.M. de Pereda, B. García-Alvarez, T. Nakamoto, B. Margolis, C.J. McGlade, R.C. Liddington, M.H. Ginsberg, Integrin beta cytoplasmic domain interactions with phosphotyrosine-binding domains: a structural prototype for diversity in integrin signaling, Proc. Natl. Acad. Sci. U. S. A. 100 (2003) 2272–2277.
[23] N.J. Anthis, J.R. Haling, C.L. Oxley, M. Memo, K.L. Wegener, C.J. Lim, M.H. Ginsberg, Campbell ID beta integrin tyrosine phosphorylation is a conserved mechanism for regulating talin-induced integrin activation, J. Biol. Chem. 284 (2009) 36,700–36,710.
[24] M. Das, S. Subbayya Ithychanda, J. Qin, E.F. Plow, Mechanisms of talin-dependent integrin signaling and crosstalk, Biochim. Biophys. Acta 2014 (1838) 579–588.
[25] E. Goksoy, Y.Q. Ma, X. Wang, X. Kong, D. Perera, E.F. Plow, J. Qin, Structural basis for the autoinhibition of talin in regulating integrin activation, Mol. Cell 11 (2008) 1124–1133.
[26] A. Bhunia, X.Y. Tang, H. Mohanram, S.M. Tan, S. Bhattacharjya, NMR solution conformations and interactions of integrin alphaLbeta2 cytoplasmic tails, J. Biol. Chem. 284 (2009) 3873–3884.
[27] O. Vinogradova, A. Velyvis, A. Velyviene, B. Hu, T. Haas, E. Plow, J.A. Qin, Structural mechanism of integrin alpha(IIb)-beta(3) "inside-out" activation as regulated by its cytoplasmic face, Cell 110 (2002) 587–597.
[28] T.S. Ulmer, D.A. Calderwood, M.H. Ginsberg, I.D. Campbell, Domain-specific interactions of talin with the membrane-proximal region of the integrin beta3 subunit, Biochemistry 42 (2003) 8307–8312.
[29] N.J. Anthis, K.L. Wegener, D.R. Critchley, I.D. Campbell, Structural diversity in integrin/talin interactions, Structure 18 (2010) 1654–1666.
[30] B. García-Alvarez, J.M. de Pereda, D.A. Calderwood, T.S. Ulmer, D. Critchley, I.D. Campbell, M.H. Ginsberg, Structural determinants of integrin recognition by talin, Mol. Cell 1 (2003) 49–58.
[31] C.G. Gahmberg, M. Grönholm, L.M. Uotila, Regulation of integrin activity by phosphorylation, Adv. Exp. Med. Biol. 819 (2014) 85–96.
[32] D. Bouvard, J. Pouwels, N. De Franceschi, J. Ivaska, Integrin inactivators: balancing cellular functions *in vitro* and *in vivo*, Nat. Rev. Mol. Cell Biol. 14 (2013) 430–442.
[33] Z. Razinia, T. Mäkelä, J. Ylänne, D.A. Calderwood, Filamins in mechanosensing and signaling, Annu. Rev. Biophys. 41 (2012) 227–246.
[34] S.S. Ithychanda, M. Das, Y.Q. Ma, K. Ding, X. Wang, S. Gupta, C. Wu, E.F. Plow, J.J. Qin, Migfilin, a molecular switch in regulation of integrin activation, J. Biol. Chem. 284 (2009) 4713–4722.
[35] S.S. Ithychanda, J. Qin, Evidence for multisite ligand binding and stretching of filamin by integrin and migfilin, Biochemistry 50 (2011) 4229–4231.
[36] J. Liu, M. Das, J. Yang, S.S. Ithychanda, V.P. Yakubenko, E.F. Plow, J. Qin, Structural mechanism of integrin inactivation by filamin, Nat. Struct. Mol. Biol. 22 (2015) 383–389.
[37] J. Yang, L. Zhu, H. Zhang, J. Hirbawi, K. Fukuda, P. Dwivedi, J. Liu, T. Byzova, E.F. Plow, J. Wu, J. Qin, Conformational activation of talin by RIAM triggers integrin-mediated cell adhesion, Nat. Commun. 5 (2014) 5880, http://dx.doi.org/10.1038/ncomms6880.
[38] C.P. Sharma, R.M. Ezzell, M.A. Arnaout, Direct interaction of filamin (ABP-280) with the beta 2-integrin subunit CD18, J. Immunol. 154 (1995) 3461–3470.
[39] M. Niki, M.K. Nayak, H. Jin, N. Bhasin, E.P. Plow, P.P. Pandolfi, P.B. Rothman, A.K. Chauhan, S.R. Lentz, Dok1 negatively regulate platelet integrin aIIbb3 outside-in signaling and inhibits thrombosis in mice, Thromb. Haemost. 115 (2016) 969-8.
[40] Y. Lad, P. Jiang, S. Ruskamo, D.S. Harburger, J. Ylänne, I.D. Campbell, D.A. Calderwood, Structural basis of the migfilin–filamin interaction and competition with integrin beta tails, J. Biol. Chem. 283 (2008) 35,154–35,163.
[41] S.S. Ithychanda, M. Das, Y.Q. Ma, K. Ding, X. Wang, S. Gupta, C. Wu, E.F. Plow, J. Qin, Migfilin, a molecular switch in regulation of integrin activation, J. Biol. Chem. 284 (2008) 4713–4722.
[42] M. Das, S.S. Ithychanda, J. Qin, E.F. Plow, Migfilin and filamin as regulators of integrin activation in endothelial cells and neutrophils, PLoS One 6 (10) (2011), e26355.
[43] G.-L. Chua, X.-Y. Tang, A.T. Patra, S.M. Tan, S. Bhattacharjya, Structure and binding interface of the cytosolic tails of αXβ2 integrin, PLoS One 7 (7) (2012), e41924, http://dx.doi.org/10.1371/journal.pone.0041924.